crystals

MDPI

Article

Complexes of Cd(II) with Nicotinamide, Nitrate, and Oxalate as Mixed Ligands: Synthesis, Characterization, and Biological Activity

Laurentiu Pricop [1], Ioana Cristina Marincas [2], Anamaria Hanganu [1], Mihaela Ganciarov [3], Augustin M. Mădălan [1] and Maria Olimpia Miclăuș [4,*]

[1] Department of Inorganic Chemistry, Organic Chemistry, Biochemistry and Catalysis, Faculty of Chemistry, University of Bucharest, 90–92 Panduri St., 050663 Bucharest, Romania; laurp2002@yahoo.com (L.P.); anamaria.hanganu@unibuc.ro (A.H.); augustin.madalan@chimie.unibuc.ro (A.M.M.)
[2] The Earth, Environmental and Life Sciences Division, The Research Institute of the University of Bucharest (ICUB), 050095 Bucharest, Romania; ioana-cristina.marinas@icub.unibuc.ro
[3] Analysis Team, National Institute for Research & Development in Chemistry and Petrochemistry—ICECHIM, Splaiul Independentei No. 202, Sector 6, 060021 Bucharest, Romania; mihaela.ganciarov@icechim.ro
[4] National Institute for R&D of Isotopic and Molecular Technologies, Donat 67-103, 5, 700, 400293 Cluj-Napoca, Romania
* Correspondence: maria.miclaus@itim-cj.ro

Abstract: Three complexes of Cd(II), $[Cd(NA)_2(NO_3)_2(H_2O)_2]$ (1), $[Cd(NA)_2(NO_3)_2(H_2O)_2]\cdot 2NA$ (2), and $[Cd(ox)(NA)(H_2O)]\cdot H_2O$ (3) (NA = nicotinamide, ox = oxalate) were synthesized and characterized. Complexes (1) and (2) are mononuclear, while complex (3) is a bidimensional polymeric coordination compound, with oxalate anions bridging metal ions in two different ways: μ_2 bis-bidentate chelating manner and μ_4 bis-bidentate bis-monodentate manner. The stereochemistry of Cd(II) in compounds (1) and (3) is a distorted pentagonal bipyramid, while in compound (2) it is a regular octahedron. Complexes (1) and (2) demonstrated significant activity against *Enterococcus faecalis* and *Escherichia coli*, showcasing their potential as effective antibacterial agents and inhibitors of microbial adhesion. The complexes were characterized by means of single-crystal X-ray diffraction, elemental analysis, FTIR (all complexes), ^{1}H NMR, ^{13}C NMR, fluorescence spectroscopy, and antimicrobial activity (complexes (1) and (2)).

Keywords: Cd(II) complexes; nicotinamide; pentagonal bipyramid geometry; hydrogen bonds

Academic Editors: Ulli Englert and Jesús Sanmartín-Matalobos

Received: 19 December 2024
Revised: 23 January 2025
Accepted: 24 January 2025
Published: 27 January 2025

Citation: Pricop, L.; Marinas, I.C.; Hanganu, A.; Ganciarov, M.; Mădălan, A.M.; Miclăuș, M.O. Complexes of Cd(II) with Nicotinamide, Nitrate and Oxalate as Mixed Ligands: Synthesis, Characterization and Biological Activity. *Crystals* **2025**, *15*, 140. https://doi.org/10.3390/cryst15020140

1. Introduction

Nicotinamide is the main form of vitamin B3, together with nicotinic acid and nicotinamide riboside [1]. All of these molecules, together with the amino acid tryptophan, are precursors of nicotinamide adenine dinucleotide (NAD^+), a coenzyme that is synthesized most easily, in only two steps, from nicotinamide [2,3]. In turn, NAD^+ is the precursor of another important coenzyme, nicotinamide adenine dinucleotide phosphate ($NADP^+$), with the two coenzymes differing by a phosphate group, provided by an ATP molecule [4]. NAD^+ plays an important role in catabolic reactions, such as glycolysis, the Krebs cycle, and oxidative phosphorylation [5,6]. On the other hand, the $NADP^+$/NADPH couple is involved in anabolic processes, such as the biosynthesis of

nucleic acids and fatty acids, while NADPH is a crucial component of the cellular antioxidation systems [7]. Moreover, NADPH has an essential role in xenobiotic biotransformation via NADPH-cytochrome P450 reductase [8–10].

Accordingly, humans need an adequate daily intake of nicotinamide, which means an amount of 16 mg for men and 14 mg for women [11]. A lack of sufficient vitamin B3 in the diet leads to pellagra, a disease also called the "disease of the 3 D's" due to its characteristic symptoms: dermatitis, diarrhea, and dementia. Pellagra was first described over two centuries ago in Spain [12]. It is prevalent in malnourished populations because the primary dietary source of nicotinamide is meat and its derivatives [13]. In the USA, between 1907 and 1940, 100,000 people died from this disease [14].

On the other hand, cadmium compounds are well-known for their toxic effects. In the 1960s, the Itai-itai disease in Japan was recognized to be caused by this harmful chemical element. At the end of the last century, 410 people were diagnosed or suspected of suffering from this condition [15]. Accordingly, there has been significant interest in recent years in studying the interaction of cadmium with endogenous molecules, such as amino acids and peptides [16–18]. Some of these interactions have been studied for applications in soil remediation [19] or to estimate stability in seawater [20]. Among these studies are complexes of Cd(II) with amino acids and vitamins as mixed ligands [21,22].

Extensive studies have also been conducted on the coordination compounds formed by $Cd(NO_3)_2$ with various ligands containing N and O donor atoms. Among these, 3-aminoquinoline acts in a monodentate mode with cadmium adopting a tetrahedral geometry [23] or in a bridging mode, generating bi- or polynuclear complexes, with cadmium exhibiting a coordination number of seven in both cases [24]. Additionally, cadmium nitrate has been used as a precursor for obtaining the clathrate $[Cd(stpy)_3(NO_3)_2]\cdot 1/2$ stpy, where stpy = trans-4-styrylpyridine. The geometry of the metal ion is a pentagonal bipyramid, with nitrate groups acting in a bidentate chelating manner [25]. On the other hand, oxalate is a well-known versatile ligand, which can exhibit 17 coordination modes [26], generating a plethora of polynuclear coordination compounds, with interesting structures and promising magnetic or electrochemical properties [27]. Among them, 1D, 2D, and 3D Cd(II) polymeric complexes, with oxalate as co-ligand, were synthesized and characterized [28,29].

When integrated into complexes, nicotinamide has the potential to enhance pharmacological effect through improving metal transport and distribution to cells. Numerous investigations have demonstrated that nicotinamide-based complexes have significant antibacterial and antioxidant properties [30–33]. Furthermore, nicotinamide acts as an active component in metal complexes, enhancing interactions with enzymes and DNA [34–36]. Configurations that expose the nicotinamide ligand can further boost bioavailability, making these compounds intriguing for medicinal purposes [37].

Although not innately antibacterial, nitrate (NO_3^-) plays a vital role in metabolic pathways that create antimicrobial compounds like nitrites (NO_2^-) and nitric oxide (NO) [38–40]. Under specific physiological or environmental circumstances, these chemicals have potent antibacterial activity [41–43]. NO, produced by nitrate reduction, disrupts bacterial biofilms by altering quorum sensing (a bacterial communication mechanism essential for sessile cells) or damaging biofilm structural integrity, rendering bacteria more susceptible to antimicrobial treatments. Since biofilms are highly resistant to conventional antibiotics, nitrate-derived NO offers a valuable strategy for addressing chronic infections associated with biofilms, such as dental plaque and chronic wounds [44].

Oxalate complexes may exhibit reduced toxicity due to their high stability, which limits the release of free cadmium ions [45]. Furthermore, these complexes may have antioxidant action due to the oxalate ligand's capacity to scavenge free radicals [46,47]. In this context, we developed a synthesis strategy to obtain cadmium complexes with

nicotinamide, nitrate, and oxalate as mixed ligands. As a result, we synthesized three new coordination compounds (Scheme 1), one of which is a 2D polynuclear complex with oxalate and nicotinamide as mixed ligands. The other two are mononuclear complexes with nicotinamide and nitrate as mixed ligands, exhibiting different geometries of the metal ion and different coordination modes of the nitrate ions. The structure of complex 2 was previously reported, but the compound was not further characterized [48].

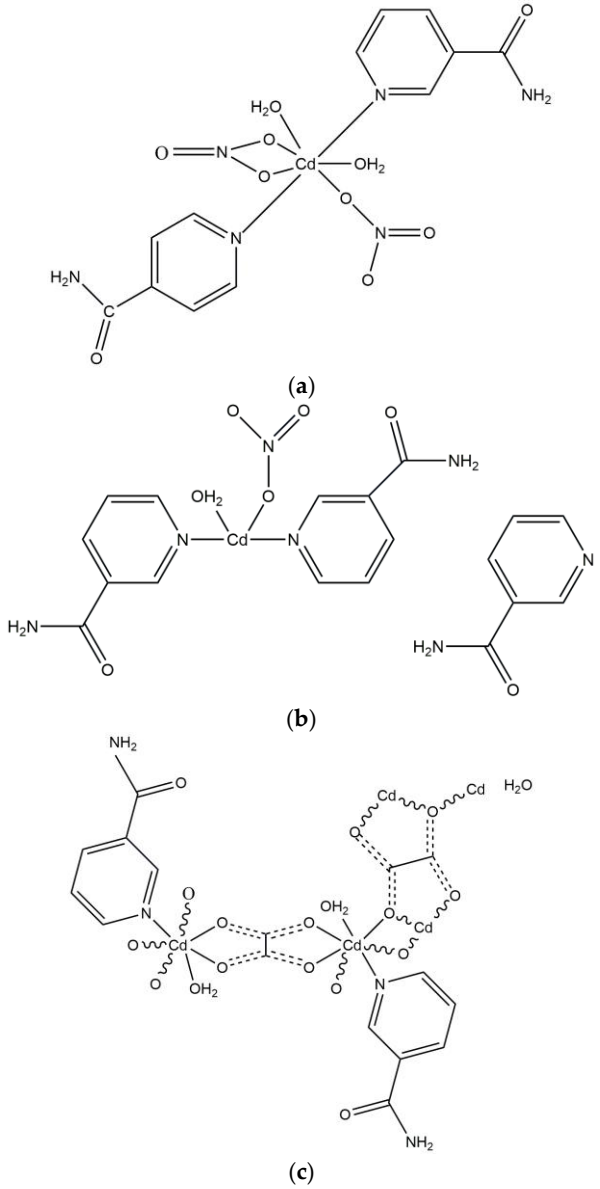

Scheme 1. Chemical diagrams of investigated complexes**:** (**a**) $[Cd(NA)_2(NO_3)_2(H_2O)_2]$**;** (**b**) $[Cd(NA)_2(NO_3)_2(H_2O)_2]\cdot 2NA$**;** (**c**) $[Cd(ox)(NA)(H_2O)]\cdot H_2O$.

2. Materials and Methods

2.1. Materials

The chemicals used for this research were purchased from Sigma-Aldrich (Darmstadt, Germany) as reagent grade and were used as received, without further purification. A FlashSmart **from** Thermo Fisher Scientific company, USA, MA, Waltham was used for chemical analyses (C, H, and N).

2.2. Synthesis of Complexes

$[Cd(NA)_2(NO_3)_2(H_2O)_2]$ (1): To a solution containing cadmium(II) nitrate tetrahydrate (0.309 g, 1 mmol) in 10 mL ethanol, a solution of nicotinamide (0.244 g, 2 mmol) dissolved in 10 mL ethanol was added. The mixture was magnetically stirred at room temperature for 3 h and then left at room temperature for slow evaporation. After a few days, white crystals suitable for X-ray analysis were obtained (0.131 g, 25.35% yield based on $Cd(NO_3)_2$. $4H_2O$).

$C_{12}H_{16}N_6O_{10}Cd$

Found (%): C, 28.54; H, 3.17; N, 16.7. Calculated (%): C, 27.88; H, 3.09; N, 16.36. IR(cm^{-1}): υ_{as} (N-H), 3376 m; υ_s (N-H), 3204 m; υ (C-H), 3075 w; υ (C-H), 2977 w; υ (C=O), 1671 s; υ (C=N), 1637 m; δ (N-H), 1596 m; υ_{as}(ONO), 1550 w; υ(C-C) + υ_{as}(ONO), 1366 vs; υ_s(ONO), 1296 vs; υ (C-NH_2), 1204 w; δ (C-H), 1141 w; δ (C-H), 1118 w; δ (C-H) + υ (C-C), 1044 m; υ (C-C), 925 w; δ (ONO), 841 w; δ (ONO), 819 w; υ (C-H), 766 m; ϱ_w (NH_2), 672 m; ϱ_w (H_2O), 572 vs; δ (C-NH_2) + γ (C=O), 492 vs.

$[Cd(NA)_2(NO_3)_2(H_2O)_2]\cdot 2NA$ (2): A mixture of cadmium(II) nitrate tetrahydrate (0.155 g, 0.5 mmol) and nicotinamide (0.244 g, 2 mmol) was dissolved in 15 mL of an ethanol–water mixture (1:1). The solution was magnetically stirred for 15 min and then refluxed for 1 h on a water bath. After filtration, the solution was left for slow evaporation, and after a few days, white crystals suitable for X-ray analysis were obtained.

An alternative synthesis was performed as follows: 0.172 g (1 mmol) of $CdCO_3$ was added to 5 mL of nitric acid solution prepared by dissolving 0.1 mL of HNO_3 (63%) in 5 mL water. To this solution, nicotinamide (0.244 g, 2 mmol) dissolved in 15 mL water was added. The mixture was stirred for 10 min at room temperature and then refluxed for 30 min. The solution was cooled and left for slow evaporation. After one week, white crystals were obtained and characterized by single-crystal X-ray diffraction, confirming the compound as $[Cd(NA)_2(NO_3)_2(H_2O)_2]\cdot 2NA$ (0.514 g, 67.54% yield, based on $Cd(NO_3)_2$. $4H_2O$).

$C_{24}H_{28}N_{10}O_{12}Cd$

Found(%): C, 37.5; H, 3.75; N, 17.67. Calculated(%): C, 37.84; H, 3.68; N, 18.39. IR(cm^{-1}): υ (O-H), 3425 m; υ_{as} (N-H), 3391 m; υ_{as} (N-H), 3309 m; υ_s (N-H), 3181 m; υ (C=O), 1667 s; υ (C=N), 1622 s; δ (N-H), 1597 s; δ (O-H), 1476 w; υ_{as}(ONO) + υ(C-C), 1390 s; υ_s(ONO), 1315 vs; υ (C-NH_2), 1200 m; δ (C-H), 1136 m; δ (C-H), 1093 w; δ (C-H) + υ (C-C), 1045 m; υ (C-C), 943 w; δ (ONO), 822 m; υ (C-H), 791 m; 748 m; ϱ_w (NH_2), 699 s; δ(CCC), 644 w; ϱ_w (H_2O), 552 vs; δ (C-NH_2) + γ (C=O), 519 vs.

$[Cd(ox)(NA)(H_2O)]\cdot H_2O$ (3): A mixture of $CdCO_3$ (0.172 g, 1 mmol) and $H_2C_2O_4\cdot 2H_2O$ (0.126 g, 1 mmol) was dissolved in 5 mL water and gently stirred for 5 min. To this solution, nicotinamide (0.122 g, 1 mmol) dissolved in 15 mL water was added. The final solution was magnetically stirred for 2 h at room temperature and then for another 15 min at 100 °C. After cooling and filtration, the solution was left at room temperature for slow evaporation. In three weeks, white crystals suitable for X-ray diffraction were separated (0.031 g, 8.64% yield based on $CdCO_3$).

$C_8H_{10}N_2O_7Cd$

Found(%): C, 27.00; H, 2.91; N, 8.21. Calculated(%): C, 26.77; H, 2.78; N, 7.80. IR (cm^{-1}): υ (O-H), 3500–3000 m; υ_{as} (N-H), 3375 m; υ_{as} (N-H), 3263 m; υ_s (N-H), 3170 m; υ_s (N-H), 3116 m; υ (C=O), 1697 vs; υ_{as} (C=O), 1663 vs; δ (O-H), 1458 w; υ_s (C=O), 1408 m; υ_s (CO) + δ(O-C=O), 1305 w; υ (C-NH_2), 1200 m; υ (C-N), 1160 w; δ (C-H), 1133 m; δ (C-H) + υ (C-C), 1040 w; υ (C-C), 949 w; υ (C-H), 807 m; ϱ_w (NH_2), 685 m; δ(CCC), 654 m; ϱ_w (H_2O), 543 m; δ (C-NH_2) + γ (C=O), 509 m.

2.3. Single Crystal X-Ray Diffraction and Refinement

The single crystals were carefully mounted on fine nylon loops coated with inert oil and positioned on the goniometer of a SuperNova diffractometer. This diffractometer is equipped with dual X-ray micro-sources (Mo and Cu), operating at 50 kV and 0.8 mA, and utilizes an Eos CCD detector. Experimental data collection, along with corrections for Lorentz, polarization, and absorption effects, was performed using the CrysAlis PRO software [49].

The structures of complexes **(**1) and **(**3) were solved using Intrinsic Phasing with the SHELXT program [50]. All structures were further refined using Least Squares with the SHELXL program [51]. All structural solutions and refinements were carried out within the Olex2 package [52].

For the refinement, hydrogen atoms bonded to carbon were located and treated as riding atoms. The isotropic displacement parameters (Uiso) for hydrogen atoms were set to 1.2 Ueq(C) for NH2 and tertiary (CH) groups, with bond lengths of 0.88 Å and 0.95 Å, respectively. OH groups were refined with Uiso = 1.5 Ueq(C) and an O-H bond length of 0.85 Å.

2.4. Fourier-Transform Infrared Spectroscopy (FT-IR)

FT-IR spectra were recorded in the range of 400–4000 cm^{-1}, using a Jasco FT-IR 4200 spectrometer coupled with **an** ATR (Pike GradiATR) unit.

2.5. Liquid Nuclear Magnetic Resonance Spectroscopy (NMR)

The NMR spectra were recorded on a Bruker Avance III Ultrashield Plus 500 MHz spectrometer, operating at 11.74 T, corresponding to the resonance frequency of 500.13 MHz for the 1H nucleus, equipped with a direct detection four**-**nuclei probe head and field gradients on the z**-**axis.

2.6. Thermogravimetric Analysis (TG)

The heating curves (TG) were recorded using a Metler Toledo TGA/SDATA 851 instrument. The measurements were carried out in synthetic air, with a heating rate of 10 K/min.

2.7. Photoluminescence

The fluorescence spectra were recorded on powder using a JASCO FP-6500 spectrofluorometer.

2.8. Elemental Analysis

A FlashSmart Thermo Fisher Scientific elemental analyzer was used for chemical analyses (C, H, and N).

2.9. Antimicrobial Activity

Qualitative assessment of antimicrobial activity: Microbial suspensions were prepared and standardized to 1.5×10^8 CFU/mL (0.5 McFarland). These suspensions were derived from 18–24 h cultures grown on solid media (Mueller–Hinton). The antimicrobial activity was evaluated using an adapted diffusion method in accordance with the CLSI (Clinical and Laboratory Standards Institute) guidelines for antibiotic activity control. The stock solutions for each compound were 10 mg/mL in DMSO. A solvent control was included for all variants. Each stock solution (10 µL) was spotted on the medium inoculated with the test strains. The formation of an inhibition zone around the sample spot on the culture medium was recorded as a positive result, and the diameters of the

inhibition zones (DIZ, mm) were measured. Reference discs used for control were as follows: kanamycin (30 μg) for Gram-positive bacteria and piperacillin (30 μg) for Gram-negative bacteria.

Quantitative assessment of antimicrobial activity was conducted using the serial two-fold microdilution method in Tryptone Soy Broth within a 96-well plate. The working concentration of stock solutions ranged between 5 and 0.08 mg/mL. Concurrently, serial dilutions in DMSO were prepared under identical conditions to serve as solvent controls for each strain. Each well received 10 μL of a microbial suspension standardized to 0.5 McFarland, derived from 18–24-h-old cultures. The negative and positive controls consisted of the culture medium (with 10 μL of NaCl 0.9%) and untreated microbial growth (with 10 μL of microbial suspension), respectively. MIC values were determined spectrophotometrically by measuring absorbance at 620 nm. The data were analyzed using the Inhibitor vs. Response analysis function in Prism GraphPad 10.0 software to calculate the IC50 (the concentration that inhibited 50% of the growth of the untreated microbial inoculum).

Evaluation of Microbicidal Activity: To determine the minimum microbicidal concentrations (MMC), 5 μL of culture from each well was plated onto agar medium. The plates were then incubated at 37 °C for 20–24 h.

Microbial Adherence: After the evaluation of MICs, microbial adherence was quantified using the *slime* method according to [53].

Statistical Analysis: Data are reported as means ± standard deviation from duplicate analyses. Statistical analysis was conducted using GraphPad Prism 10.0. Two-way ANOVA followed by Tukey's multiple comparisons test was used to evaluate the comparison between IC50 values of the samples and the solvent.

3. Results

3.1. Crystal Structures Descriptions

The detailed crystallographic and refinement data of the analyzed crystals are displayed in Table S1.

Complex (1)

Using single crystal X-ray diffraction analysis, it was found that complex (1) is mononuclear, with the asymmetric unit illustrated in Figure 1a. The complex crystallizes in the centrosymmetric P-1 space group. The coordination environment consists of one central metal atom (Cd^{2+}), two monodentate nicotinamide molecules coordinating via the N3 and N4 nitrogen atoms of the pyridine rings, one bidentate coordinated nitrate anion (NO_3^-), one monodentate coordinated nitrate anion (NO_3^-), and two water molecules from the recrystallization medium. Complex (1) is a μ_2 bis-bidentate chelating complex with a distorted pentagonal bipyramid configuration. The pyridine-to-metal distances are 2.295 Å and 2.292 Å, while the coordination distances with the nitrate anion are 2.442 Å and 2.656 Å. The metal-to-water molecule distances are 2.306 Å and 2.335 Å, respectively.

The cohesion within the crystal lattice is driven by a combination of O-H···O, N-H···O, and C-H···O hydrogen bonds, where the water molecules, the NH_2 groups of the amide, and CH groups of the phenyl rings act as donors, while the nitrate anions and the two oxygen atoms of the amide groups serve as hydrogen bond acceptors (Table S2). An overall crystal packing diagram of complex (1) is depicted in Figure 1b.

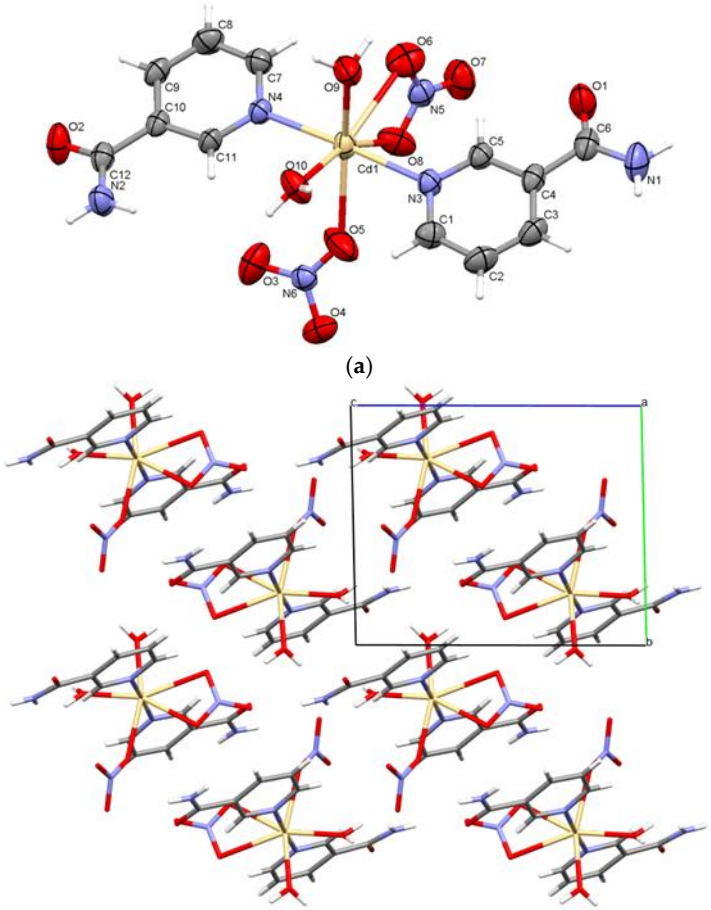

(**a**)

(**b**)

Figure 1. Asymmetric unit of complex (1) illustrating the atoms as thermal ellipsoids at a 50% probability level (**a**); unit cell packing along a-axis (**b**).

Complex (3)

Complex (3) crystallizes in the centrosymmetric P-1 space group of the triclinic crystal system. The asymmetric unit consists of one metal cation (Cd^{2+}), one nicotinamide molecule coordinated to the metal via the N1 nitrogen of the pyridine ring, two water molecules, and two halves of oxalate anions coordinated to the metal via O2 and O4. The overall coordination environment in complex (3) is characterized by two metal centers adopting a bidimensional polymeric coordination configuration, with oxalate anions bridging the metal cations in two different ways: μ_2 bis-bidentate chelating and μ_4 bis-bidentate bis-monodentate (Figure 2a).

In the direction of the b-axis, the oxalate anions and both water molecules, via O-H···O hydrogen bonding, serve as bridges in coordination, forming infinite chains (Figure 2b). These chains are extended and linked to parallel chains located one unit cell away in the direction of the c-axis via combinations of N-H···O and C-H···O intermolecular interactions, where the amide and CH groups of the pyridine rings act as hydrogen bond donors, while the oxygen atoms of the oxalate anions serve as acceptors. It is worth noting that the stability is further enhanced by π···π interactions (3.199 and 3.357 Å) which take place between pyridine rings (Table S2).

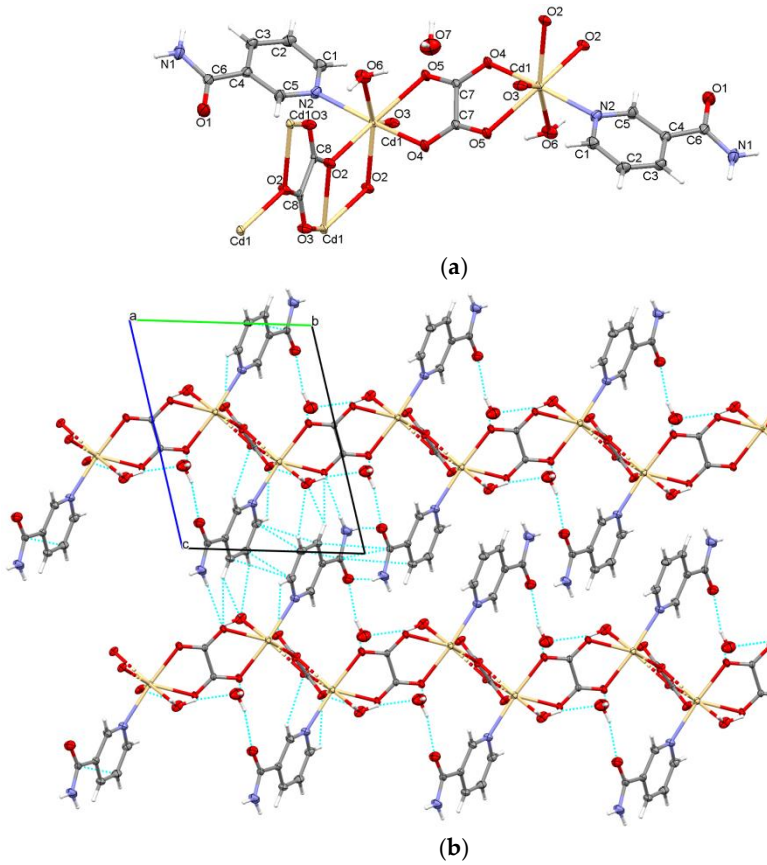

(**a**)

(**b**)

Figure 2. Coordination environment in complex (3) (**a**); crystal packing along oa-axis and intermolecular interactions (**b**).

3.2. FT-IR Spectroscopy

The spectra of complexes (1) and (2) exhibit broad bands between 3600 and 3000 cm^{-1}, assigned to the υ (O-H) vibrations of the coordinated water molecules. Additionally, the wagging vibrations, recorded as strong bands at 580–550 cm^{-1}, belong to these molecules.

The peaks at 3376 and 3204 cm^{-1} in the spectrum of complex (1) are due to asymmetrical and symmetrical N–H stretching vibrations. For complex (2), the spectrum reveals two asymmetrical valence vibrations specific to the N–H bonds of the amido group, at 3391 and 3309 cm^{-1}. These correspond to the two types of nicotinamide molecules in the complex—uncoordinated and coordinated to the metal ion. Furthermore, the N–H in-plane bending vibration appears as a strong band at 1596–1597 cm^{-1}.

The absorptions observed at 1620–1640 cm^{-1} are assigned to υ (C=N) vibrations from the pyridinic ring of the nicotinamide molecules [54]. In both spectra, very strong bands characteristic of the symmetric stretching vibration of the nitrate group are detected. They appear at 1296 cm^{-1} in complex (1) and at 1315 cm^{-1} in the spectrum of complex (2).

For complex (2), the band of the asymmetric valence vibration υ_{as} (ONO) probably overlaps with the strong band at 1390 cm^{-1}, while the band due to δ (ONO) vibration appears at 822 cm^{-1}. In the spectrum of complex (1), two coordination modes of the nitrate group are observed: monodentate and chelating bidentate. At 1550 cm^{-1}, the band of υ_{as} (ONO) of the chelating nitrate was identified, while the similar ban for the monodentate group overlaps with that of the υ (C-C) vibration, resulting in the very strong absorption at 1366 cm^{-1}. This assignment is consistent with the much smaller difference $\Delta = \upsilon_{as}$ (ONO)—υ_{s} (ONO) specific to the monodentate coordination mode versus the chelating bidentate one. Additionally, at 841 and 819 cm^{-1}, two characteristic bands of the δ (ONO) vibrations of the two differently coordinated nitrate groups were identified [25,55].

The IR spectrum of complex (3) shows characteristic bands of υ (O-H) valence vibrations (3500–3000 cm^{-1}), υ_{as} (N–H) and υ_{s} (N–H) vibrations, appearing at 3375 cm^{-1} and 3263 cm^{-1}, and at 3170 cm^{-1} and 3116 cm^{-1}, respectively. The presence of the oxalate group in the complex is supported by the very strong band at 1663 cm^{-1}, corresponding to υ_{as} (C=O) stretching vibrations, and the bands at 1408 cm^{-1} and 1309 cm^{-1}, attributed to υ_{s} (C=O) and υ_{s} (C=O) + δ (O-C=O) vibrations [55].

In addition to the broad band from 3500 to 3000 cm^{-1}, the existence of water molecules is confirmed by the peak at 543 cm^{-1}, attributed to ϱw (H_2O).

3.3. Liquid Nuclear Magnetic Resonance Spectroscopy (NMR)

^{1}H-NMR (500 MHz, DMSO-d6, δ ppm, J Hz): 9.02 (s, 2H, H-1), 8.69 (d, 2H, H-5, 4.0 Hz), 8.21 (dt, 2H, H-3, 1.8 Hz, 7.9 Hz), 8.16 (s, 2H, NH2), 7.59 (s, 2H, NH2), 7.50 (dd, 2H, H-4, 4.9 Hz, 7.7 Hz) ppm.

^{13}C-NMR (125 MHz, DMSO-d6, δ ppm): 166.4, 151.8, 148.7, 135.3, 129.7, 123.5 ppm.

$[Cd(NA)_2(NO_3)_2(H2O)_2].2NA$ (2)

^{1}H-NMR (500 MHz, DMSO-d6, δ ppm, J Hz): 9.02 (d, 4H, H-1, 1.8 Hz), 8.69 (dd, 4H, H-5, 1.5 Hz, 4.8 Hz), 8.21 (dt, 4H, H-3, 1.8 Hz, 7.9 Hz), 8.16 (s, 4H, NH2), 7.60 (s, 4H, NH2), 7.50 (dd, 4H, H-4, 4.8 Hz, 7.8 Hz) ppm.

^{13}C-NMR (125 MHz, DMSO-d6, δ ppm): 166.4, 151.8, 148.7, 135.3, 129.7, 123.5 ppm.

The ^{1}H-NMR and ^{13}C–NMR spectrums of compound $[Cd(NA)_2(NO_3)_2(H_2O)_2].2NA$ are prezented in Figures S1 and S2. Figure 3 shows the structure of nicotinamide and the numbering of its atoms, while the ^{1}H NMR spectrum of complex (1) is shown in Figure 4.

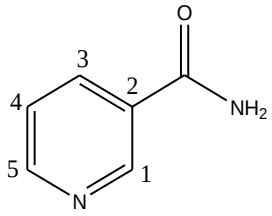

Figure 3. Chemical structure of nicotinamide.

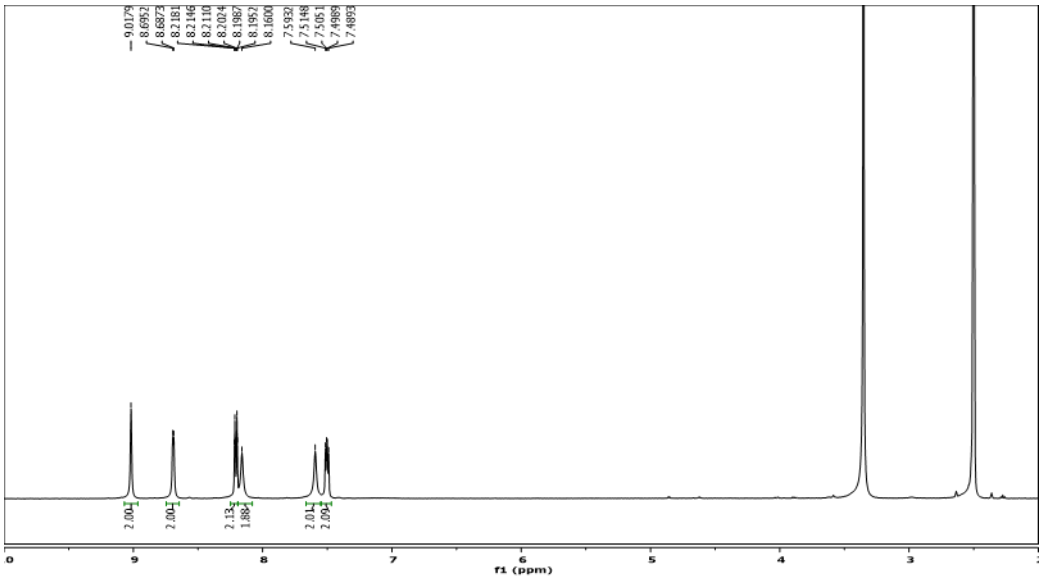

Figure 4. ^{1}H NMR spectrum of the complex **$[Cd(NA)_2(NO_3)_2(H2O)_2]$**.

Complexes (1) and (2) exhibit signals at six different positions in the range of chemical shifts δ ~ 9 to 7.5 ppm. The protons from the amino group are non-equivalent

and they are observed around 8.2 and 7.6 ppm, while the protons from the aromatic ring of nicotinamide appear at about 9.0, 8.7, 8.2, and 7.5 ppm. In complex (2), all the protons from the two types of nicotinamide are magnetically equivalent, and that is why only six signals appeared in the carbon spectrum.

3.4. Thermogravimetric Analysis

The TG curves of complexes (1) and (2) were recorded up to 900 °C. Both of them show four weight loss steps. In complex **(1)**, the first step of decomposition takes place in the range of 75–190 °C and is caused by the elimination of the coordinated water molecules (found = 6.42%; calculated = 6.96%). The second step (190–330 °C) corresponds to the loss of both nicotinamide molecules (found/calculated = 46.2%/47.2%), while the third and the fourth step are recorded in the ranges of 330–390 °C and 390–520 °C. They correspond to the elimination of nitrate groups (23.92 found/23.99 calculated). The residue of decomposition is the metal oxide. The thermogram of complex (1) is presented below in Figure 5.

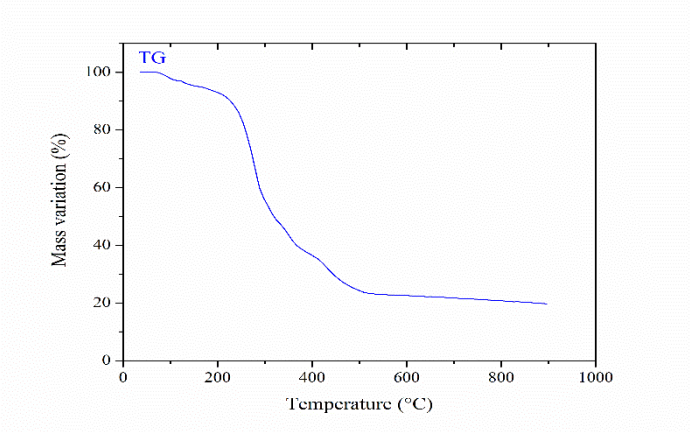

Figure 5. The TG curve of complex (1).

Complex (2) decomposes in four steps as well. The first (105–190 °C) is due to the loss of the two coordinated water molecules (5.25%—found, 4.73%—calculated). The following stages take place in the temperature ranges of 190–290 °C and 290–370 °C, respectively, and they are probably due to the loss of the coordinated and lattice nicotinamide molecules (Figure S3). The last step of decomposition is recorded in the range of 370–520 °C and corresponds to the elimination of nitrate groups. The residue consists of CdO and, probably, residual carbon.

3.5. Photoluminescence

The room temperature photoluminescence of compound (1) was explored using excitation wavelengths from the 290–320 nm range. The emission spectrum obtained by excitation at 300 nm displays an asymmetric band with maxima at 415 nm and a "shoulder" at around 468 nm (Figure 6). Because d^{10} metal ions are usually not oxidized or reduced, the observed peaks probably originate in intraligand transitions. The band with *a* maximum at 415 nm could be assigned to a $\pi^* \rightarrow \pi$ transition, while the shoulder is attributable to a $\pi^* \rightarrow$ n transition. This is a feature of the excitation spectra characteristic of heterocyclic ligands with nitrogen atoms [56,57]. Complex **(2)** was also tested, but it does not show luminescence properties.

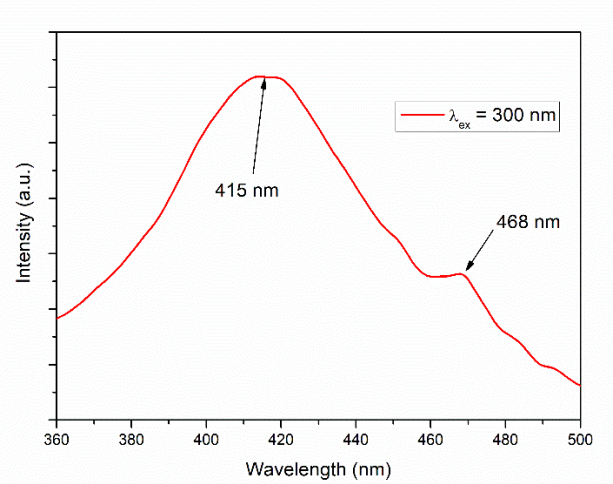

Figure 6. The solid-state emission spectrum for the compound (**1)** obtained by excitation at 300 nm.

Photoluminescence is an important feature for biologically active compounds since it has several applications in monitoring, detecting, and assessing their interactions in biological contexts. This feature can assist in analyzing the compound's behavior in various conditions, offering information into the degree of solubility, stability, and distribution in an in vitro or in vivo model [58,59].

3.6. Antimicrobial Investigation

The antimicrobial activity for compound 3 was not assessed due to its inability to solubilize in DMSO and its sensitivity to structural changes.

The evaluation of qualitative antimicrobial activity provides an initial indication of a compound's ability to inhibit microbial growth, serving as an important stage in the discovery of new antibacterial agents. These qualitative tests allow for a rapid assessment of the spectrum of antimicrobial activity. Table 1 displays the (DIZ) for each sample. The largest inhibition zone was observed for *the* sample of complex (2) against the *E. coli* strain, while the most active compound against *S. aureus* was (1).

For all samples, the (DIZ) were significantly larger than those of the solvent control (DMSO, $p < 0.0001$). However, none of the samples demonstrated activity against the *E. faecalis* strain (Figure 7). This suggests that the antimicrobial activity is more effective against Gram-negative bacteria. Hydrophobic compounds may have limited diffusion due to lower solubility in the agar medium, potentially leading to smaller inhibition zones even if the compound has significant antimicrobial activity. Hydrophobic compounds are generally more effective in penetrating microbial cell membranes, particularly those of Gram-negative bacteria, which have outer membranes rich in lipopolysaccharides [60,61]. This could explain the enhanced activity against Gram-negative strains.

Table 1. The results of the qualitative testing of antimicrobial activity on strains of *S. aureus*, *E. faecium*, *E. coli*, and *P. aeruginosa*.

Sample	*S. aureus*	*E. faecalis*	*E. coli*	*P. aeruginosa*
(2)	7.50 ± 0.58	0.00 ± 0.00	9.50 ± 0.58	5.75 ± 0.96
(1)	8.00 ± 1.41	0.00 ± 0.00	9.00 ± 1.41	6.5 ± 1.00
Kanamycine (K)	24.67 ± 0.58	16.33 ± 0.58	-	-
Piperacillin (PRL)	-	-	22.33 ± 0.58	12.00 ± 1.00
DMSO	3.50 ± 0.71	0.00 ± 0.00	0.00 ± 0.00	0.00 ± 0.00

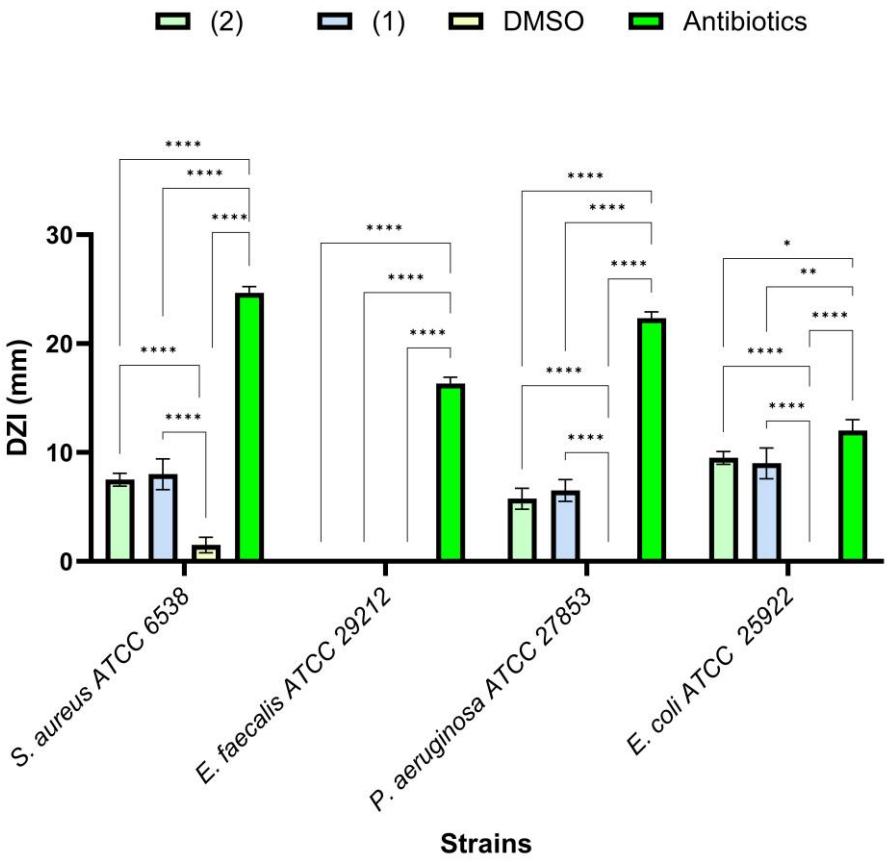

Figure 7. Comparative qualitative evaluation of antibacterial activity between samples and the solvent (DMSO) against microbial strains (* $p < 0.05$, ** $p < 0.01$, **** $p < 0.0001$).

In Table 2, the quantitative parameters of antimicrobial activity are summarized. The sample of complex (2) was particularly effective against the *E. faecalis*, *E. coli*, and *P. aeruginosa* strains, with a MIC of 0.625 mg/mL, which was lower than that of the solvent control. Similarly, the sample of complex (1) exhibited higher activity against *E. faecalis* (0.3125 mg/mL) and *P. aeruginosa* (0.625 mg/mL) strains.

The efficacy of complexes (1) and (2) may be attributed to their molecular structures, which likely contain functional groups or features that facilitate interaction with microbial cell components, such as the cell wall, membrane, or essential enzymes. Notably, the minimum microbicidal concentration (MMC) was lower than that of the solvent control only for Gram-positive bacteria.

Statistical analysis of IC50 values revealed no significant differences between complexes (1) and (2) ($p > 0.05$), though both exhibited significantly higher antimicrobial activity compared to DMSO ($p < 0.0001$; Figure 8). The antimicrobial activity against the tested strains followed the following order: *S. aureus* < *E. coli* < *P. aeruginosa* < *E. faecalis*. The discrepancies between the diffusion and microdilution methods highlight the influence of compound properties (e.g., hydrophobicity, diffusion capacity) and bacterial cell wall structure on antimicrobial activity. For *E. faecalis*, the lack of observable activity in the diffusion test underscores the limitations of agar-based methods for hydrophobic compounds, while the enhanced activity in microdilution reflects their true potential when diffusion barriers are removed [62,63].

Table 2. The quantitative evaluation of antimicrobial activity expressed by the minimum inhibitory concentration (MIC), the minimum microbicidal concentration (MMC), and the concentration required to reduce microbial viability by 50% (IC50).

	Analytical Parameter	*S. aureus ATCC 6538*	*E. faecalis ATCC 29212*	*E. coli ATCC 25922*	*P. aeruginosa ATCC 27853*
(2)	MIC (mg/mL)	1.25	0.625	0.625	0.625
	MMC (mg/mL)	2.5	5	2.5	2.5
	IC50 (mg/mL)	0.636 ± 0.077	0.059 ± 0.006	0.282 ± 0.031	0.294 ± 0.006
(1)	MIC (mg/mL)	1.25	0.3125	1.25	0.625
	MMC (mg/mL)	2.5	5	2.5	2.5
	IC50 (mg/mL)	0.601 ± 0.034	0.1057 ± 0.016	0.325 ± 0.062	0.297 ± 0.008
DMSO	MIC (mg/mL)	2.5	2.5	2.5	1.25
	MMC (mg/mL)	5	>5	2.5	2.5
	IC50 (mg/mL)	1.608 ± 0.004	0.968 ± 0.069	0.642 ± 0.006	0.524 ± 0.024

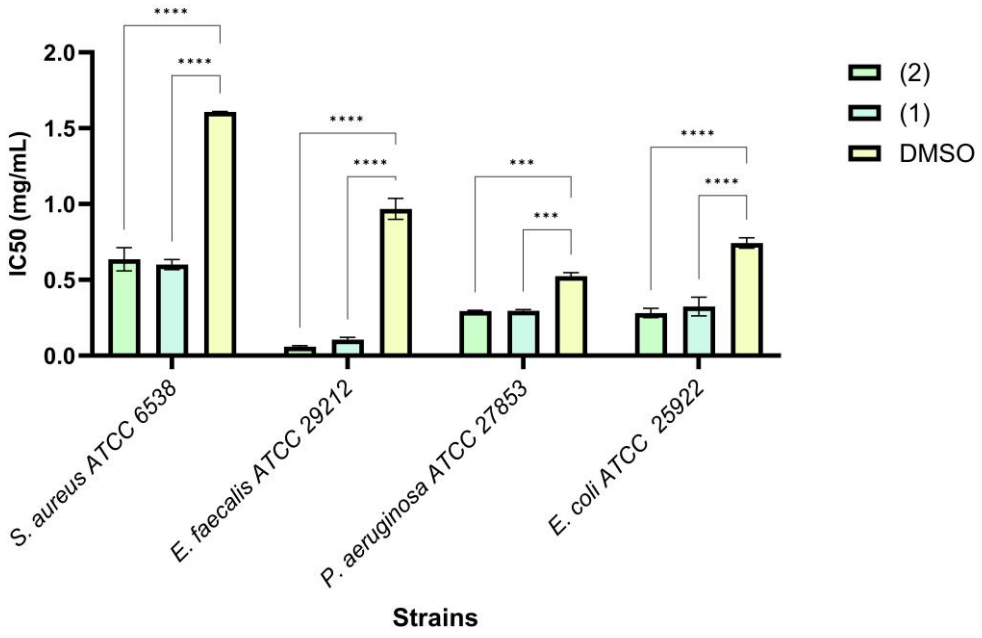

Figure 8. Antimicrobial activity expressed as IC50 and the correlation with the solvent activity used against Gram-positive and Gram-negative bacteria strains (*** $p < 0.01$, **** $p < 0.0001$).

The IC50 values obtained for complexes (1) and (2) demonstrate significant antimicrobial activity compared to DMSO, emphasizing that they are directly involved in the bacteria growth. The observed variances between bacterial strains are related to structural differences, such as cell wall thickness or resistance mechanisms, and the chemical characteristics of the complexes, such as hydrophobicity [64].

The microdilution method for establishing IC50 values gives a more precise assessment of antibacterial activity by eliminating the diffusion challenges seen in agar-based approaches. Despite the lack of apparent action in diffusion tests, the low IC50 values for *E. faecalis* demonstrate the compounds' significant therapeutic potential. Gram-positive bacteria, such as E. faecalis, have a thick peptidoglycan-rich cell wall, which allows some chemicals, particularly metal complexes, to pass through more readily. This permeability may explain *E. faecalis*' sensitivity (low IC50). The differences between *S. aureus* and *E. faecalis* are most likely related to alterations in peptidoglycan thickness or

plasma membrane composition, both of which are somewhat affected by the chemical structure of the complexes [65].

Gram-negative bacteria, on the other hand, have a more complicated cell wall structure, including an outer membrane rich in lipopolysaccharides (LPSs), which serves as a barrier to many antimicrobial drugs. *E. coli* was more susceptible among Gram-negative bacteria strains than *P. aeruginosa*, most likely due to variations in membrane composition. *P. aeruginosa* possesses a more efficient efflux pump mechanism and a more impermeable membrane barrier, which help it tolerate antimicrobial drugs. *E. coli* has a more porous and sensitive membrane than other Gram-positive bacteria, although it is still more resistant [66,67].

The impact of the newly synthesized compounds against microbial adhesion, the first stage of biofilm growth, was also assessed. The MBEC values are provided in Table 3 The compounds with MBEC values lower than their MIC values were considered effective in inhibiting microbial adhesion. However, none of the compounds demonstrated a reduction in microbial adherence at concentrations below their MIC values. The fact that none of the compounds reduced microbial adhesion at concentrations below their MIC values suggests that their anti-adhesive activity is closely linked to their antimicrobial activity. This implies that the compounds likely disrupt microbial adhesion by interfering with cell viability, rather than by targeting specific adhesion processes [68].

Table 3 indicates that the MBEC values for all strains, except *E. coli*, were lower for both samples compared to the solvent control. For the *E. coli* strain, the sample of complex **(1)** showed the same effect as DMSO (highlighted in blue in Table 3).

Table 3. Minimum concentration for inhibiting microbial adhesion to an inert substrate (blue—$MBEC_{sample} < MBEC_{DMSO}$).

	(2)		**(1)**		**DMSO**	
	MIC (mg/mL)	**MBEC (/mL)**	**MIC (/mL)**	**MBEC (/mL)**	**MIC (/mL)**	**MBEC (/mL)**
S. aureus ATCC 6538	1.25	1.25	1.25	1.25	2.5	2.5
E. faecalis ATCC	0.625	0.625	0.3125	0.3125	2.5	2.5
E. coli ATCC 11229	0.625	0.625	1.25	1.25	2.5	1.25
P. aeruginosa ATCC 27853	0.625	0.625	0.625	0.625	1.25	1.25

These complexes' antibacterial activities are strongly related to how they interact with bacteria. Nicotinamide enhances the interaction of these complexes with bacterial DNA due to its aromatic structure [69], effectively inhibiting DNA replication and bacterial growth.

4. Conclusions

Three new complexes of Cd (II) with nicotinamide, nitrate, and oxalate as mixed ligands have been synthesized and characterized by means of elemental analysis, single crystal X-ray diffraction, thermogravimetric analysis, and photoluminescence properties. All complexes were tested for their antibacterial activity. The results of the antimicrobial study suggest that the newly synthesized compounds exhibit promising antimicrobial activity, particularly against Gram-negative bacteria. Their hydrophobicity may enhance their ability to interact with microbial membranes. The compounds also showed potential to affect microbial adhesion, although this effect appears to be related to their overall antimicrobial activity. Future studies should focus on further exploring their mechanisms of action and potential therapeutic applications.

Supplementary Materials: The following supporting information can be downloaded at: https://www.mdpi.com/article/10.3390/cryst15020140/s1, Figure S1: ^{1}H-NMR spectrum of compound $[Cd(NA)_2(NO_3)_2(H_2O)_2].2NA$; Figure S2: ^{13}C-NMR spectrum of compound $[Cd(NA)_2(NO_3)_2(H_2O)_2].2NA$; Figure S3: TG curve of complex $[Cd(NA)_2(NO_3)_2(H_2O)_2].2NA$; Table S1: Crystal data and refinement details; Table S2: Hydrogen bond geometry for Complex I. and Complex III (Å, º). CIF files of the structures were deposited by the Cambridge Crystallographic Data Centre: 2411414. (Complex (1)); 2411416 (Complex (3)). The copies can be obtained free of charge on written application to CCDC, 12 Union Road, Cambridge, CB2 1EZ, UK (fax: +44-1223 336033); or by access to http://www.ccdc.cam.ac.uk (26 January 2025).

Author Contributions: Conceptualization, M.O.M. and L.P.; methodology, L.P. and I.C.M.; software, M.O.M. and I.C.M.; validation, L.P., A.H., A.M.M., I.C.M., and M.G.; investigation, L.P., A.H., A.M.M., I.C.M., M.O.M., and M.G.; writing—original draft preparation, M.O.M. and L.P.; writing—review and editing, M.O.M. All authors have read and agreed to the published version of the manuscript.

Funding: This This research was funded by PN 23.06 and PN 23.04.05 Core Program—ChemNewDeal within the National Plan for Research, Development and Innovation 2022–2027, developed with the support of the Ministry of Research, Innovation, and Digitization.

Data Availability Statement: The original contributions presented in this study are included in the article/supplementary material. Further inquiries can be directed to the corresponding author.

Conflicts of Interest: The authors declare no conflicts of interest.

References

1. Conze, D.; Crespo-Barreto, J.; Kruger, C. Safety Assessment of Nicotinamide Riboside, a Form of Vitamin B$_3$. *Hum. Exp. Toxicol.* **2016**, *35*, 1149–1160. https://doi.org/10.1177/0960327115626254.
2. Cantó, C.; Menzies, K.J.; Auwerx, J. NAD+ Metabolism and the Control of Energy Homeostasis: A Balancing Act between Mitochondria and the Nucleus. *Cell Metab.* **2015**, *22*, 31–53. https://doi.org/10.1016/j.cmet.2015.05.023.
3. Xiao, W.; Wang, R.-S.; Handy, D.E.; Loscalzo, J. NAD(H) and NADP(H) Redox Couples and Cellular Energy Metabolism. *Antioxid. Redox Signal.* **2018**, *28*, 251–272. https://doi.org/10.1089/ars.2017.7216.
4. Hoxhaj, G.; Ben-Sahra, I.; Lockwood, S.E.; Timson, R.C.; Byles, V.; Henning, G.T.; Gao, P.; Selfors, L.M.; Asara, J.M.; Manning, B.D. Direct Stimulation of NADP$^+$ Synthesis through Akt-Mediated Phosphorylation of NAD Kinase. *Science* **2019**, *363*, 1088–1092. https://doi.org/10.1126/science.aau3903.
5. Yang, Y.; Sauve, A.A. NAD + Metabolism: Bioenergetics, Signaling and Manipulation for Therapy. *Biochim. et Biophys. Acta (BBA)-Proteins Proteom.* **2016**, *1864*, 1787–1800. https://doi.org/10.1016/j.bbapap.2016.06.014.
6. Sauve, A.A. NAD$^+$ and Vitamin B$_3$: From Metabolism to Therapies. *J. Pharmacol. Exp. Ther.* **2008**, *324*, 883–893. https://doi.org/10.1124/jpet.107.120758.
7. Ying, W. NAD$^+$/NADH and NADP$^+$/NADPH in Cellular Functions and Cell Death: Regulation and Biological Consequences. *Antioxid. Redox Signal.* **2008**, *10*, 179–206. https://doi.org/10.1089/ars.2007.1672.
8. Gan, L.; Von Moltke, L.L.; Trepanier, L.A.; Harmatz, J.S.; Greenblatt, D.J.; Court, M.H. Role of NADPH-Cytochrome P450 Reductase and Cytochrome- *b*$_5$/NADH- *b*$_5$ Reductase in Variability of CYP3A Activity in Human Liver Microsomes. *Drug Metab. Dispos.* **2009**, *37*, 90–96. https://doi.org/10.1124/dmd.108.023424.
9. Smith, L.L. Paraquat Toxicity. *Phil. Trans. R. Soc. Lond. B* **1985**, *311*, 647–657. https://doi.org/10.1098/rstb.1985.0170.
10. *Casarett & Doull's Essentials of Toxicology*; Klaassen, C.D., Watkins, J.B., Casarett, L.J., Doull, J., Eds.; 4th ed.; McGraw Hill: New York, NY, USA, 2021; ISBN 978-1-260-45229-7.
11. Fessel, J.P.; Oldham, W.M. Pyridine Dinucleotides from Molecules to Man. *Antioxid. Redox Signal.* **2018**, *28*, 180–212. https://doi.org/10.1089/ars.2017.7120.
12. Hegyi, J.; Schwartz, R.A.; Hegyi, V. Pellagra: Dermatitis, Dementia, and Diarrhea. *Int. J. Dermatol.* **2004**, *43*, 1–5. https://doi.org/10.1111/j.1365-4632.2004.01959.x.

13. Çatak, J. Determination of Niacin Profiles in Some Animal and Plant Based Foods by High Performance Liquid Chromatography: Association with Healthy Nutrition. *J. Anim. Sci. Technol.* **2019**, *61*, 138–146. https://doi.org/10.5187/jast.2019.61.3.138.
14. Morabia, A. Joseph Goldberger's Research on the Prevention of Pellagra. *J. R. Soc. Med.* **2008**, *101*, 566–568. https://doi.org/10.1258/jrsm.2008.08k010.
15. Nishijo, M.; Nakagawa, H.; Suwazono, Y.; Nogawa, K.; Kido, T. Causes of Death in Patients with Itai-Itai Disease Suffering from Severe Chronic Cadmium Poisoning: A Nested Case–Control Analysis of a Follow-up Study in Japan. *BMJ Open* **2017**, *7*, e015694. https://doi.org/10.1136/bmjopen-2016-015694.
16. Sóvágó, I.; Várnagy, K. Cadmium(II) Complexes of Amino Acids and Peptides. In *Cadmium: From Toxicity to Essentiality*; Sigel, A., Sigel, H., Sigel, R.K., Eds.; Metal Ions in Life Sciences; Springer: Dordrecht, The Netherlands, 2013; Volume 11, pp. 275–302. ISBN 978-94-007-5178-1.
17. Bottari, E.; Festa, M.R. Asparagine as a Ligand for Cadmium(II), Lead(II) and Zinc(II). *Chem. Speciat. Bioavailab.* **1996**, *8*, 75–83. https://doi.org/10.1080/09542299.1996.11083272.
18. Kozłowski, H.; Urbańska, J.; Sóvágó, I.; Varnagy, K.; Kiss, A.; Spychała, J.; Cherifi, K. Cadmium Ion Interaction with Sulphur Containing Amino Acid and Peptide Ligands. *Polyhedron* **1990**, *9*, 831–837. https://doi.org/10.1016/S0277-5387(00)81348-0.
19. Yao, W.; Yang, Z.; Huang, L.; Su, C. Complexation of Amino Acids with Cadmium and Their Application for Cadmium-Contaminated Soil Remediation. *Appl. Sci.* **2022**, *12*, 1114. https://doi.org/10.3390/app12031114.
20. Simões^Gonçalves, M.L.S.; Correia Dos Santos, M.M. Cadmium Complexes of Aminoacids in Seawater Conditions. *J. Electroanal. Chem. Interfacial Electrochem.* **1984**, *163*, 315–326. https://doi.org/10.1016/S0022-0728(84)80059-5.
21. Zhang, F.; Liu, Q. Ternary Complexes of Cadmium(II) with Vitamin D_3 and Aminoacids: Quantitative Expressions of Relative Stabilities. *J. Coord. Chem.* **1993**, *28*, 197–202. https://doi.org/10.1080/00958979308037097.
22. Khan, F.; Khanam, A. Study of Complexes of Cadmium with Some L-Amino Acids and Vitamin-C by Voltammetric Technique. *Eclet. Quím.* **2008**, *33*, 29–36. https://doi.org/10.1590/S0100-46702008000200004.
23. Azam, M.; Al-Resayes, S.I.; Pallepogu, R. Synthesis and Structural Characterization of Cadmium(II) and Mercury(II) Complexes Derived from 3-Aminoquinoline. *Helv. Chim. Acta* **2016**, *99*, 20–23. https://doi.org/10.1002/hlca.201500164.
24. Kovalev, V.V.; Kokunov, Y.V.; Shmelev, M.A.; Voronina, Y.K.; Kiskin, M.A.; Popov, L.D.; Eremenko, I.L. Molecular and Polymeric Cadmium Nitrate Complexes with Bridging 3-Aminoquinoline: Synthesis, Structures, and Luminescence Properties. *Russ. J. Coord. Chem.* **2021**, *47*, 272–279. https://doi.org/10.1134/S1070328421040047.
25. Karunakaran, C.; Thomas, K.R.J.; Asurname, A.; Murugesan, R. Synthesis, Structure and Spectroscopy of Clathrate Inclusion Compounds of Cobalt(II), Cadmium(II) and Zinc(II) Trans-4-Styrylpyridine Nitrates as Host with Trans-4-Styrylpyridine as Guest (2:1)[No Title Found]. *J. Incl. Phenom. Macrocycl. Chem.* **2000**, *38*, 233–249. https://doi.org/10.1023/A:1008137311908.
26. Rao, C.N.R.; Natarajan, S.; Vaidhyanathan, R. Metal Carboxylates with Open Arhitectures. *Angew. Chem. Int. Ed.* **2004**, *43*, 1466–1496, doi.org/10.1002/anie.200300588.
27. Clulow, R.; Lightfoot, P. Syntheses and crystal structures of three novel oxalate coordination compounds: $Rb_2Co(C_2O_4)_2{\cdot}4H_2O$, $Rb_2CoCl_2(C_2O_4)$ and $K_2Li_2Cu(C_2O_4)_3{\cdot}2H_2O$. *Acta Crystallogr. E Crystallogr. Comm.* **2023**, *79*, 267–271.
28. Xia, S.-Q.; Hu, S.-M.; Dai, J.-C.; Wu, X.-T.; Fu, Z.-Y.; Zhang, J.-J.; Du, W.-X. Syntheses and structures of 1D, 2D, 3D cadmium (II) coordination polymers with oxalate and aromatic co-ligands. *Polyhedron* **2004**, *23*, 1003–1009, doi.org/10.1016/j.poly.2003.12.021.
29. Dey, S.K.; Shyamapada, S.; Sankolli, R., Guru Row, T.N. A new 3D cadmium (II) coordination polymer having μ_4-oxalato, μ-aquo and μ-chlorido bridges: Crystal structure, solid state fluorescence and thermal behavior. *J. Mol. Struct.* **2013**, *1048*, 6–10, doi.org/10.1016/j.molstruc.2013.05.018.
30. de Oliveira Neto, J.G.; Rodrigues, A.O.J.; Viana, R.J.; Barros, D.S.J.; Lage, R.M.; de Sousa, F.F.; Dutra, R.P.; Souto, E.B.; dos Santos, A.O. Antibacterial $[Zn(nicotinamide)_2Cl_2]$ complex for the treatment of skin conditions: An experimental-theoretical study of physicochemical, microbiological and in silico pharmacokinetic properties. *J. Mol. Liq.* **2024**, *403*, 124846, doi.org/10.1016/j.molliq.2024.124846.
31. Altun, O.; Suozher, M. Synthesis, spectral analysis, stability constants, antioxidant and biological activities of Co(II), Ni(II) and Cu(II) mixed ligand complexes of nicotinamide, theophylline and thiocyanate. *J. Mol. Struct.* **2017**, *1149*, 307–314, doi.org/10.1016/j.molstruc.2017.07.069.
32. Yıldırım, T.; Köse, D.A.; Avcı, E.; Özer, D.; Şahin, O. Novel mixed ligand complexes of acesulfame/nicotinamide with some transition metals. Synthesis, crystal structural characterization, and biological properties. *J. Mol. Struct.* **2019**, *1176*, 576–582, doi.org/10.1016/j.molstruc.2018.08.099.

33. Moncol, J.; Kuchtanin, V.; Polakovičová, P.; Mroziński, J.; Kalińska, B.; Koman, M.; Padělková, Z.; Segl'a, P.; Melník, M. Study of copper(II) thiophenecarboxylate complexes with nicotinamide. *Polyhedron* **2012,** *45*, 94–102, doi.org/10.1016/j.poly.2012.07.069.
34. Rendošová, M.; Vargová, Z.; Kuchár, J.; Sabolová, D.; Levoča, S.; Kudláčová, J.; Paulíková, H.; Hudecová, D.; Helebrandtová, V.; Almáši, M.; et al. New silver complexes with bioactive glycine and nicotinamide molecules–Characterization, DNA binding, antimicrobial and anticancer evaluation. *J. Inorg. Biochem.* **2017**, *168*, 1–12, doi.org/10.1016/j.jinorgbio.2016.12.003.
35. Kalaivanan, C.; Sankarganesh, M.; Yosuva Suvaikin, M.; Banu Karthi, G.; Gurusamy, S.; Subramanian, R.; Nandini Asha, R. Novel Cu(II) and Ni(II) complexes of nicotinamide based Mannich base: Synthesis, characterization, DFT calculation, DNA binding, molecular docking, antioxidant, antimicrobial activities. *J. Mol. Liq*, **2020**, *320*, 114423, doi.org/10.1016/j.molliq.2020.114423.
36. Al-Saif, F.A.; Refat, S.M. Ten metal complexes of vitamin B3/niacin: Spectroscopic, thermal, antibacterial, antifungal, cytotoxicity and antitumor studies of Mn(II), Fe(III), Co(II), Ni(II), Cu(II), Zn(II), Pd(II), Cd(II), Pt(IV) and Au(III) complexes. *J. Mol. Struct*. **2012**, *1021*, 40–52, doi.org/10.1016/j.molstruc.2012.04.057.
37. Ban, E.; An Hyeon, S.; Park, B.; Park, M.; Yoon, N.-E.; Jung, B.H.; Kim, A. Improved Solubility and Oral Absorption of Emodin-Nicotinamide Cocrystal Over Emodin with PVP as a Solubility Enhancer and Crystallization Inhibitor. *J. Pharm. Sci.* **2020**, *109*, 3660–3667, doi.org/10.1016/j.xphs.2020.09.030.
38. Zhao, Y.; Chen, Z.; Wang, Q.; Zhang, C.; Ji, M. A new insight to explore toxic Cd(II) affecting denitrification: Reaction kinetic, electron behavior and microbial community. *Chemosphere* **2022**, *305*, 135419, doi.org/10.1016/j.chemosphere.2022.135419.
39. Singh, S.; Anil, G.A.; Kumar, V.; Kapoor, D.; Subramanian, S.; Singh, J.; Ramamurthy, P.C. Nitrates in the environment: A critical review of their distribution, sensing techniques, ecological effects and remediation. *Chemosphere* **2022**, *287*, 131996, doi.org/10.1016/j.chemosphere.2021.131996.
40. Wang, X.; Du, H.; Ma, M.; Rennenberg, H. The dual role of nitric oxide (NO) in plant responses to cadmium exposure. *Sci.Total Environ*. **2023**, *892*, 164597, doi.org/10.1016/j.scitotenv.2023.164597.
41. Rosier, B.T.; Buetas, E.; Moya-Gonzalvez, E.M.; Artacho, A.; Mira, A. Nitrate as a potential probiotic for the oral microbiom. *Sci. Rep.* **2020**, *10*, 12895, doi.org/10.1038/s41598-020-69931-x.
42. Tiso, M.; Schechter, A.N. Nitrate reduction to nitrite, nitric oxide and ammonia by gut bacteria under physiological conditions. *PLoS ONE* **2015**, *10*, e0119712, doi.org/10.1371/journal.pone.0127490.
43. Okda, M.; Spina, S.; Fakhr, B.S.; Carroll, R.W. The Antimicrobial Effects of Nitric Oxide: A Narrative Review. *Nitric Oxide* **2025**, doi.org/10.1016/j.niox.2025.01.001.
44. Majou, D.; Christieans, S. Mechanisms of the bactericidal effects of nitrate and nitrite in cured meats. *Meat Sci.* **2018**, *145*, 273–284, doi.org/10.1016/j.meatsci.2018.06.013.
45. Steckerman, T.; Thomine, S. Mechanisms of Cadmium Accumulation in Plants. *Crit. Rev. Plant. Sci.* **2020**, *39*, 322–359, doi.org/10.1080/07352689.2020.1792179.
46. Thamilselvan, S.; Khan, S.R.; Menon, M. Oxalate and calcium oxalate mediated free radical toxicity in renal epithelial cells: Effect of antioxidants. *Urol. Res.* **2003**, *31*, 3–9. doi.org/10.1007/s00240-002-0286-x.
47. Selasteen, F.D.; Raj S, A.C. In vitro study of antimicrobial and antioxidant activities of oxalic acid-derived bioactive chelating agent. *Asian J. Pharm. Clin. Res.* **2019**, *12*, 423-427. https://doi.org/10.22159/ajpcr.2019.v12i2.29193.
48. Lian, Z.; Zhao, N.; Yang, F.; Liu, P. Crystal structure of trans-trans-trans-diaquabis(nicotinamide)-dinitratocadmium(II)-nicotinamide (1:2), $Cd(H_2O)_2(C_6H_6N_2O)_2(NO_3)_2.2C_6H_6N_2O$. *Z. Kristallogr. NCS* **2011**, *226*, 289–290, doi.org/10.1524/ncrs.2011.0128.
49. CrysAlis PRO 2018. Available online: https://rigaku.com/products/crystallography/x-ray-diffraction/crysalispro (accessed on 23 January 2025).
50. Sheldrick, G.M. *SHELXT*–Integrated Space-Group and Crystal-Structure Determination. *Acta Crystallogr. A Found. Adv.* **2015**, *71*, 3–8. https://doi.org/10.1107/S2053273314026370.
51. Sheldrick, G.M. Crystal Structure Refinement with *SHELXL*. *Acta Crystallogr. C Struct. Chem.* **2015**, *71*, 3–8. https://doi.org/10.1107/S2053229614024218.
52. Dolomanov, O.V.; Bourhis, L.J.; Gildea, R.J.; Howard, J.A.K.; Puschmann, H. *OLEX2*: A Complete Structure Solution, Refinement and Analysis Program. *J. Appl. Crystallogr.* **2009**, *42*, 339–341. https://doi.org/10.1107/S0021889808042726.
53. Corbu, V.M.; Georgescu, A.-M.; Marinas, I.C.; Pericleanu, R.; Mogos, D.V.; Dumbravă, A.Ș.; Marinescu, L.; Pecete, I.; Vassu-Dimov, T.; Czobor Barbu, I.; et al. Phenotypic and Genotypic Characterization of Resistance and Virulence Markers in *Candida* spp. Isolated from Community-Acquired Infections in Bucharest, and the Impact of AgNPs on the Highly Resistant Isolates. *J. Fungi* **2024**, *10*, 563. doi.org/10.3390/jof10080563.

54. Ramalingam, S.; Periandy, S.; Govindarajan, M.; Mohan, S. FT-IR and FT-Raman vibrational spectra and molecular structure investigation of nicotinamide: A combined experimental and theoretical study. *Spectrochim. Acta A Mol. Biomol. Spectrosc.* **2010**, *75*, 1552–1558.
55. Nakamoto, K. *Infrared and Raman Spectra of Inorganic and Coordination Compounds, Part B–Applications in Coordination, Organometallic, and Bioinorganic Chemistry*, 6th ed.; John Wiley & Sons, Inc.: Hoboken, NJ, USA, 2009; pp. 221–227.
56. He, C.J.; Wang, Y.F.; Li, S.H. Hydrothermal Syntheses, Crystal Structures and Luminescence Properties of Two Cadmium (II) Complexes Based on 3-Hydroxyisonicotinic Acid. *Russ. J. Gen. Chem.* **2024**, *94*, 1412–1418, doi.org/10.1134/S1070363224060185.
57. Marcenko, R.D.; Lysova, A.A.; Samsonenko, D.G.; Dybtsev, D.N.; Potapov, A.S. Synthesis, structural diversity, luminescent properties and antibacterial effects of cadmium (II) and silver (I) coordination compounds with bis(1,2,3-benzotriazol-1-yl)alkanes. *Polyhedron* **2020**, *177*, 114330, doi.org/10.1016/j.poly.2019.114330.
58. Sun, M.; Mullen, K.; Yin, M. Water-soluble perylenediimides: Design concepts and biological applications. *Chem. Soc. Rev.* **2016**, *45*, 1513–1528, doi.org/10.1039/C5CS00754B.
59. Monteiro, J.H.S.K. Recent Advances in Luminescence Imaging of Biological Systems Using Lanthanide(III) Luminescent Complexes. *Molecules* **2020**, *25*, 2089, doi.org/10.3390/molecules25092089.
60. Alkarri, S.; Bin Saad, H.; Soliman, M. On Antimicrobial Polymers: Development, Mechanism of Action, International Testing Procedures, and Applications. *Polymers* **2024**, *16*, 771. https://doi.org/10.3390/polym16060771.
61. Delcour, A.H. Outer Membrane Permeability and Antibiotic Resistance. *Biochim. et Biophys. Acta (BBA)-Proteins Proteom.* **2009**, *1794*, 808–816. https://doi.org/10.1016/j.bbapap.2008.11.005.
62. Hossain, T.J. Methods for Screening and Evaluation of Antimicrobial Activity: A Review of Protocols, Advantages, and Limitations. *EuJMI* **2024**, *14*, 97–115. https://doi.org/10.1556/1886.2024.00035.
63. Balouiri, M.; Sadiki, M.; Ibnsouda, S.K. Methods for in Vitro Evaluating Antimicrobial Activity: A Review. *J. Pharm. Anal.* **2016**, *6*, 71–79. https://doi.org/10.1016/j.jpha.2015.11.005.
64. Nawrocki, K.L.; Crispell, E.K.; McBride, S.M. Antimicrobial Peptide Resistance Mechanisms of Gram-Positive Bacteria. *Antibiotics* **2014**, *3*, 461–492, doi.org/10.3390/antibiotics304046.
65. Nikolic, P.; Mudgil, P. The Cell Wall, Cell Membrane and Virulence Factors of *Staphylococcus aureus* and Their Role in Antibiotic Resistance. *Microorganisms* **2023**, *11*, 259. https://doi.org/10.3390/microorganisms11020259.
66. Chevalier, S.; Bouffartigues, E.; Bodilis, J.; Maillot, O.; Lesouhaitier, O.; Feuilloley, M.G.J.; Orange, O.; Dufour, A.; Cornelis, P. Structure, function and regulation of *Pseudomonas aeruginosa* porins. *FEMS Microbiol. Rev.* **2017**, *41*, 698–722, doi.org/10.1093/femsre/fux020.
67. Antonelli, G.; Cappelli, L.; Cinelli, P.; Cuffaro, R.; Manca, B.; Nicchi, S.; Tondi, S.; Vezzani, G.; Viviani, V.; Delany, I.; et al. Strategies to Tackle Antimicrobial Resistance: The Example of *Escherichia coli* and *Pseudomonas aeruginosa*. *Int. J. Mol. Sci.* **2021**, *22*, 4943. https://doi.org/10.3390/ijms22094943.
68. Uzoma, P.C.; Etim, I.-I.N.; Okonkwo, B.O.; Olanrele, O.S.; Njoku, D.I.; Kolawole, S.K.; Emori, W.; Ikeuba, A.I.; Njoku, C.N.; Ekerenam, O.O.; et al. Recent Design Approaches, Adhesion Mechanisms, and Applications of Antibacterial Surfaces. *Chem. Eng. J. Adv.* **2023**, *16*, 100563. https://doi.org/10.1016/j.ceja.2023.100563.
69. Surendra Dilip, C.; Siva Kumar, V.; John Venison, S.; Vetha potheher, I.; Rajalaxmi (a) Subahashini, D. Synthesis, structural characterisation, bio-potential efficiency and DNA cleavage applications of nicotinamide metal complexes. *J. Mol. Struct.* **2013**, *1040*, 192–205, doi.org/10.1016/j.molstruc.2013.02.019.